

# **ScienceDirect**



IFAC PapersOnLine 58-28 (2024) 887-892

# LiFePO<sub>4</sub> Battery Thermal Modeling: Bus Bar Thermal Effects \*

Meridian Haas\* Alireza Nemati\* Scott Moura\*\* Shima Nazari\*

\* Mechanical and Aerospace Engineering Department, University of California, Davis, CA 95616 USA (emails: mhaas@ucdavis.edu, nemati@ucdavis.edu, snazari@ucdavis.edu) \*\* Civil and Environmental Engineering Department, University of California, Berkeley, CA 94720 USA (email: smoura@berkeley.edu).

Abstract: Lithium iron phosphate (LFP) batteries are ideal for electrification of off-road heavy-duty vehicles with less concerns on the system weight. However, the limited battery life aggravated by the long working hours is a primary concern for some off-road applications such as construction equipment. Temperature is one of the main influencing factors in battery aging. Therefore, accurate prediction of temperature dynamics with fast lumped parameter models is essential and can be used for long-term analysis. This paper introduces a thermal model for pack of cells, with each cell represented by surface and core temperature states. We derived model parameters from experimental thermal cycling data, emphasizing the significance of reversible entropic heat generation for capturing faster dynamics. Furthermore, our work highlights the errors introduced by neglecting the bus bar thermal effects when extending a single-cell model to a cell pack. Our proposed solution incorporates the conduction between cell cores via the bus bar and accounts for heat dissipation through convection from the bus bar to surrounding air.

Copyright © 2024 The Authors. This is an open access article under the CC BY-NC-ND license (https://creativecommons.org/licenses/by-nc-nd/4.0/)

Keywords: Lithium-ion battery, battery pack, thermal modeling, physics-based modeling, control-oriented modeling.

### 1. INTRODUCTION

Lithium-ion batteries fueled the movement toward vehicle electrification. On-road electric vehicles typically run on lithium nickel cobalt aluminum oxide (NCA) or lithium nickel manganese cobalt oxide (NMC) batteries. However, electrifying off-road vehicles presents unique challenges for which NCA and NMC batteries are unsuitable. Off-road vehicles often incorporate lithium iron phosphate (LiFePO<sub>4</sub>, LFP) batteries which are less energy dense compared to the other chemistries; however, they typically have a longer lifetime and lower risk of thermal runaway [Camargos et al. (2022)]. These properties make LFP batteries the ideal candidate for heavy-duty off-road applications in which weight is not a significant concern. Understanding the behavior of LFP batteries is essential for widespread adoption.

Control-oriented battery modeling with simple dynamic equations allows for efficient simulation for control, estimation, and long-term studies. Thermal modeling, which predicts the temperature evolution of the battery cells over time is critical as temperature is a key factor in battery aging [Wang et al. (2011)]. Recently, two-state thermal models have been developed with the lumped-parameter approach for LFP cells. Forgez et al. (2010) and Barbieri et al. (2022) estimate the model's parameters by assuming constant heat generation and analyzing the steady state operation but more accuracy can be found by parameter-

izing the model through least-squares optimization as in Perez et al. (2012).

In a battery pack, cells next to one another are connected electrically in series and parallel with bus bars. To convert cell-level thermal models to describe full battery operation, many models will assume that there is a large enough gap that the cells do not directly exchange heat and only dissipate heat to the cooling media [He et al. (2023)]. Bus bar effects are almost always neglected in control-oriented models, and only more complex models that describe the temperature with detailed partial differential equations (PDEs) include the bus bar effects [Chen et al. (2023)]. Only Fan et al. (2014) have included bus bar convection and conduction in a control-oriented model of a composite LMO-NMC battery, however, they describe each cell with a single temperature state. There is still a gap for thermal models that are simple enough for fast simulation but capture the complexity of the thermal behavior of the battery, including the bus bar effect.

This paper presents a simple thermal model for LFP battery packs that captures cell-to-cell interactions and bus bar effects. The model has been parameterized through detailed experimental analysis. In this work, we emphasize that the faster thermal dynamics of the battery cells can only be captured by including the entropic heat generation, which is often neglected in battery thermal modeling. Furthermore, we show that including the bus bar thermal effects results in far more accurate battery pack modeling.

 $<sup>^{\</sup>star}\,$  This research was sponsored by CITRIS and the Banatao Institute.

The rest of this paper is organized as follows: Section 2. presents the experimental setup, Section 3. describes the equivalent circuit model, and Section 4. details the thermal model for a single cell and then the development and parameterization of the thermal model for connecting cells in parallel.

#### 2. EXPERIMENTAL SETUP

The specifications of the prismatic LFP cells that are studied here are provided in Table 1.

Table 1. The specifications of the studied cells.

Category	Value
Chemistry	${ m LiFePO_4}$
Model	Fortune 32250322
Capacity	25  Ah
Nominal Voltage	$3.2~\mathrm{V}$
Cell Dimensions (LxWxH)	$70~\mathrm{mm} \times 27~\mathrm{mm} \times 165~\mathrm{mm}$
Cell Mass	$625~\mathrm{g}$
Bus Bar Dimensions (LxWxt)	$45~\mathrm{mm} \times 15~\mathrm{mm} \times 0.5~\mathrm{mm}$
Bus Bar Mass	$2.50 \; { m g}$

An Arbin Instruments LBT20 Battery Tester was used to conduct the experiments. K-type thermocouples measured the temperature of different parts of the cell as shown in Fig. 1. The surface temperature can easily be measured, however, the temperature of the center of the battery is inaccessible. In this work, we approximated the temperature of the core with the terminal temperature similar to Barbieri et al. (2022). The battery thermal model is coupled with its electrical model, as the heat generation within a cell is driven by the internal resistance. Therefore, the next section provides the parameterization of the electrical model, and then the thermal model is presented.

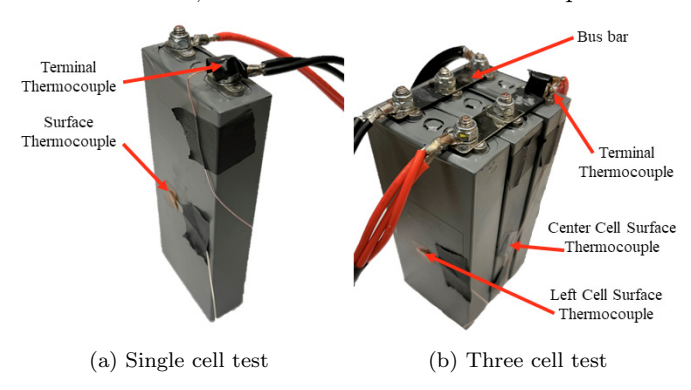


Fig. 1. Experimental setup with thermocouples placed to measure the surface and terminal temperatures (a) for single cell experiments and (b) for 3 cell experiments.

## 3. BATTERY ELECTRICAL MODEL

This section details the parameterization of the electrical model of the studied LFP prismatic cell. The battery cell's state of charge (SOC) can be calculated using the Coulomb counting method

$$\frac{dSOC}{dt} = \frac{I}{3600C_{bat}} \tag{1}$$

where I is the current applied to the cell, with a positive current corresponding to charging the battery, and  $C_{bat}$  is battery's nominal capacity in Ampere-hours (Ah).

An Equivalent Circuit Model (ECM) is often used to describe the electrical dynamics of the LFP prismatic battery cell. An ECM relates the operation of the cell to an electrical circuit with components such as a voltage source, resistors, and capacitors. Hu et al. (2009) have shown an ECM with two resistor capacitor (RC) pairs can emulate the dynamics of an LFP cell, so this paper uses the 2-RC ECM as shown in Fig. 2.

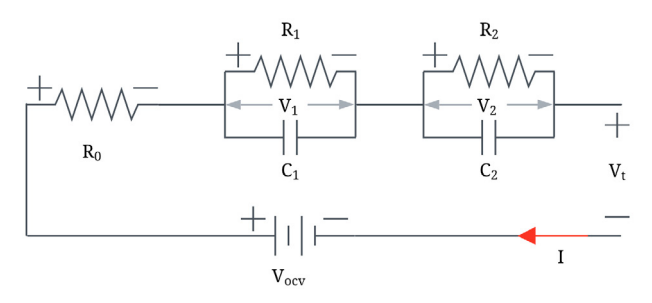


Fig. 2. Equivalent circuit model describing the electrical dynamics of the cell with 2 RC pairs.

The voltage dynamics for the ECM are described as

$$\frac{dV_1}{dt} = -\frac{V_1}{R_1C_1} + \frac{I}{C_1} 
\frac{dV_2}{dt} = -\frac{V_2}{R_2C_2} + \frac{I}{C_2} 
V_t = V_{ocv} + V_1 + V_2 + IR_0$$
(2)

where  $V_1$  and  $V_2$  are the voltages across the two RC components with the resistors  $R_1$  and  $R_2$  and capacitors  $C_1$  and  $C_2$ , respectively. The terminal voltage,  $V_t$ , depends on the open circuit voltage,  $V_{ocv}$ , the internal resistance,  $R_0$ , and the RC voltages. The parameterization of the electrical model begins with determining  $V_{ocv}$ . To do so, the battery was fully discharged and charged at a low crate (C/20) with the Arbin Battery Tester. Assuming the value of the  $V_{ocv}$  is independent of charging or discharging and ignoring the effects of hysteresis, the average voltage response then represents the  $V_{ocv}$  of the cell.

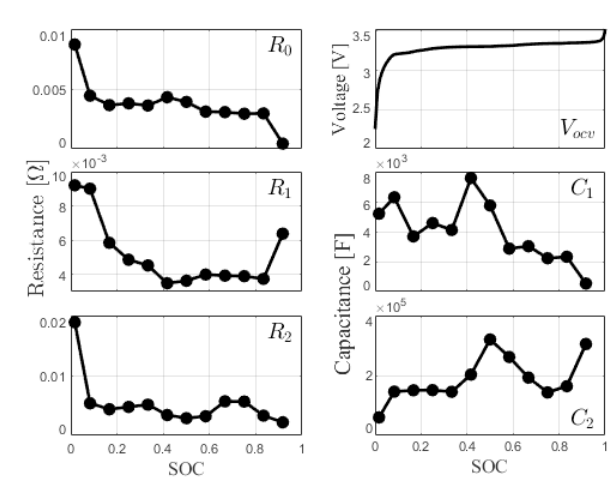


Fig. 3. Battery electrical model parameters based on SOC found through least squared error curve fit.

The values of the other parameters in the electrical model, denoted as  $P_e = [R_0, R_1, C_1, R_2, C_2]$ , depend on the SOC and the cell temperature. However, since this study is focused on thermal modeling and the temperature deviations

during the tests were less than  $10^{o}C$ , this parameterization was only done once at room temperature. To find these constants at different SOCs, the battery cell underwent 12 pulses at 1 c-rate (25A). The set of ordinary differential equations in (2) can be solved analytically, first for the pulse and then the relaxation as in Perez et al. (2012). The results for the electrical parameters are depicted in Fig. 3.

#### 4. BATTERY THERMAL MODEL

This section develops a thermal model of the LFP battery with prismatic cells. The single cell thermal model and its parameterization are provided first. The impact of entropic heat generation is highlighted and supported by experiments in the next part. A multi-cell thermal model is introduced, and finally the influence of the bus bars and a method for modeling the thermal effects of bus bars are presented.

We performed thermal cycling of the cells by charging and discharging the battery with 20A until the temperature reached steady state. The current and voltage profiles for these experiments are shown in Fig. 4.

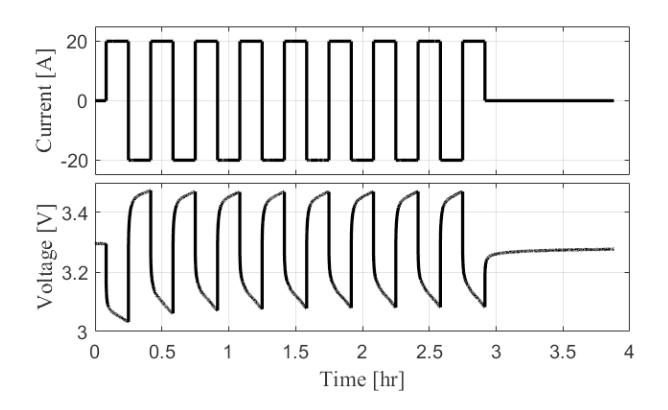


Fig. 4. Thermal Cycling: Induced current and corresponding voltage response used to determine the temperature dynamics of the cells.

### 4.1 Single Cell Thermal Model

A single cell thermal model is developed based on the conventional lumped capacitance approximation. The model has two states: the core temperature and the surface temperature. The entire surface is approximated to be at the same temperature since it is composed of aluminum, which has a high thermal conductivity. Our experiments found the average temperature difference between thermocouples placed on various faces of the cell was 0.123  $\Delta^oC$ .

Heat generated in the core of the cell is dissipated to the surface through conduction, while the surface of the cell is exposed to still air, which cools the surface with convection. The effects of convection within the cell and radiation are negligible, therefore, the thermal dynamics of the two states can be described by

$$C_c \frac{dT_c}{dt} = \dot{Q} + \frac{T_s - T_c}{R_c}$$

$$C_s \frac{dT_s}{dt} = \frac{T_c - T_s}{R_c} + \frac{T_a - T_s}{R_a}$$
(3)

where  $T_c$  and  $T_s$  are the core and surface temperatures, respectively, and  $\dot{Q}$  is the rate of heat generated in the battery.  $C_c$  and  $C_s$  are the thermal capacitances of the core and surface of the battery, while  $R_c$  is the thermal resistance to conduction within the battery and  $R_a$  is the thermal resistance to convection with the surrounding air at a temperature of  $T_a$ .

The largest contribution to the rate of heat generated in the cell is irreversible heat generation from the energy dissipated from electrode overpotentials and joule heating. The total heat generation is often approximated with only the rate of irreversible heat generation [Perez et al. (2012)]

$$\dot{Q} \approx \dot{Q}_{irr} = I(V_t - V_{ocv}) \ . \tag{4}$$

To find the parameters for the lumped parameter model, we discretized (3) using the Euler approximation with a time step,  $\Delta t$ , of one second as follows

$$\begin{bmatrix} T_c \\ T_s \end{bmatrix}_{k+1} = A_d \begin{bmatrix} T_c \\ T_s \end{bmatrix}_k + \begin{bmatrix} \frac{\Delta t}{C_c} & 0 \\ 0 & \frac{\Delta t}{R_c C_c} \end{bmatrix} \begin{bmatrix} \dot{Q} \\ T_a \end{bmatrix}_k$$
 (5)

in which

$$A_d = \begin{bmatrix} 1 - \frac{\Delta t}{R_c C_c} & \frac{\Delta t}{R_c C_c} \\ \frac{\Delta t}{R_c C_s} & 1 - \frac{\Delta t (R_a + R_c)}{R_c R_a C_s} \end{bmatrix} . \tag{6}$$

The thermal parameters,  $P_t = [C_c, R_c, C_s, R_a]$ , are optimized to minimize the error between the model and data at each time step, i, for both the surface and the core temperature

$$P_{t}^{*} = \underset{P_{t}}{\operatorname{argmin}} \sum_{i=1}^{n} (T_{c,model}(i, P_{t}) - T_{c,data}(i))^{2} + \omega \sum_{i=1}^{n} (T_{s,model}(i, P_{t}) - T_{s,data}(i))^{2}.$$
(7)

The relative weighting between the surface and core temperature errors is denoted  $\omega$ , with a value of 2 as the core temperature measurement is an approximation. The minimization is solved with Matlab's *fminsearch*. The results of this parameterization for one representative thermal cycling test are given in Fig. 5.

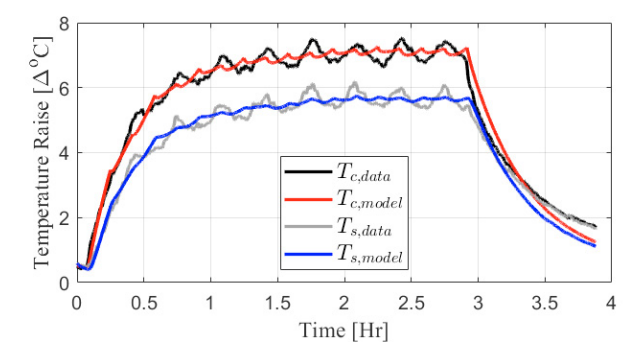


Fig. 5. Single cell thermal model from (4)-(6). RMSE is  $0.1303~\Delta^o C$  for  $T_c$  and  $0.1106~\Delta^o C$  for  $T_s$ , excluding the period of relaxation.

Although the model can predict the average temperature rise, it is evident per Fig. 5 that the model fails to capture the faster dynamics of the cell temperature. After a careful

investigation, it was discovered the reason lies with the simplification of the heat generation model and neglecting the reversible heat generation term.

# 4.2 Entropic Heat Generation

Bernardi et al. (1985) described the rate of heat generated in the cell through chemical reaction with both irreversible and reversible terms as

$$\dot{Q} = \dot{Q}_{irr} + \dot{Q}_{rev} \ . \tag{8}$$

The reversible heat generation,  $\dot{Q}_{rev}$ , is based on the heat generated from enthalpy change

$$\dot{Q}_{rev} = T\Delta S \frac{I}{F} \tag{9}$$

where  $\Delta S$  is the entropy change during the reaction, and F is the Faraday constant. The change in entropy is proportional to the change in Gibbs free energy,  $\Delta G$ , and change in temperature. The open circuit voltage is proportional to the Gibbs free energy, Faraday constant, and n, the number of electrons exchanged during the reaction.

$$\Delta S = -\frac{\partial \Delta G}{\partial T} = nF \frac{\partial V_{ocv}}{\partial T} \ . \tag{10}$$

There is one electron exchanged in the battery reaction, thus, the reversible heat generated in the cell is

$$\dot{Q}_{rev} = IT \frac{\partial V_{ocv}}{\partial T} \ . \tag{11}$$

 $\partial V_{ocv}/\partial T$  is called the entropic coefficient and is typically determined by varying the temperature of the cell and measuring the resulting change to  $V_{ocv}$ . Mendoza and Fathy (2014) and Forgez et al. (2010) have found the relation for cylindrical 18650 and 26650 LFP cells, respectively, and Bazinski and Wang (2013) measured the entropic coefficient for a 14Ah LFP prismatic cell. The results of these studies are compared in Fig. 6.

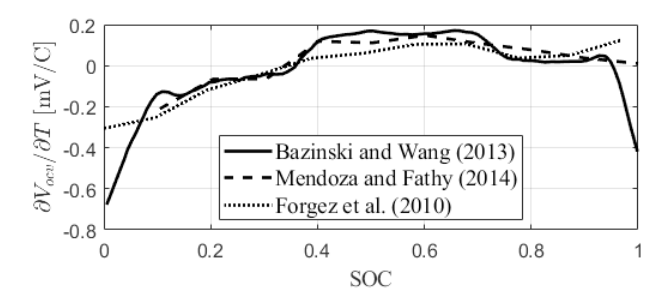


Fig. 6. Entropic coefficients determined by Bazinski and Wang (2013), Mendoza and Fathy (2014), and Forgez et al. (2010).

The models generally agree, however, since the cell in Bazinski and Wang (2013) is the closest in size and shape to our 25Ah prismatic cell and has the highest data resolution, the results of this study are used to approximate  $\partial V_{ocv}/\partial T$  for our thermal model. The model is parameterized by solving (7) and Fig. 7 depicts the resulting model.

It is clear that the addition of the entropic heat generation allows the model to fully capture the uneven heating of the cell during charge and discharge when the initial SOC is close to 0.5. For tests that began with the cell at a higher SOC, the entropic heat generation instead resulted

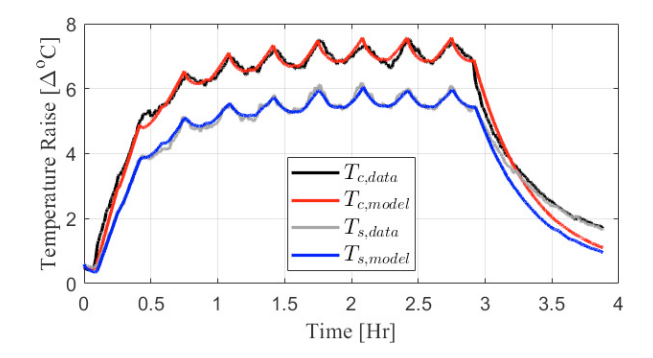


Fig. 7. Single cell thermal model results including the entropic generation term. RMSE is 0.0955  $\Delta^o C$  for  $T_c$  and 0.0522  $\Delta^o C$  for  $T_s$ , excluding the period of relaxation.

in a more uniform heat generation across the charging and discharging cycling. The errors in the model during the thermal relaxation period are attributed to the increased air temperature around the battery, which the thermocouple farther from the cell's surface underestimates. The identified model parameters and their respective physical counterparts are given in Table 2.

Table 2. Cell-level thermal model parameters.

Parameters					
$R_c$	$0.4690 \; \mathrm{K/W}$	k	2.4922 W/(m·K)		
$R_a$	$1.7281 \; K/W$	h	$17.0699 \text{ W/(m}^2 \cdot \text{K)}$		
$C_c$	653.6069  J/K	Cp	1184.1  J/(kg·K)		
$C_s$	122.3806  J/K	$t_s$	1.418 mm		

Our identified parameters are all within the range reported in literature. For example, the found specific heat, Cp, is close to the number reported by Sheng et al. (2019) for LFP prismatic cells. Converting their in-plane estimate of thermal conductivity to represent the total cell thermal conductivity, k, yields values that verify our results. The convective heat transfer coefficient of air, h, and the thickness of the shell,  $t_s$ , are close to the typical reported values (10-100 W/(m<sup>2</sup>·K), 1.1 mm).

#### 4.3 Multi-Cell Thermal Model

Two different tests were performed to isolate the thermal effects of the bus bar from the heat transfer between the cells: one with the cells connected in parallel and another with the cells in the same position but connected to 3 separate channels. The bus bars limit the placement of the cells such that they can be fully in contact or have a maximum gap of 4 mm between the cells. Two tests were done with the cells in each of the four configurations described in Fig. 8.

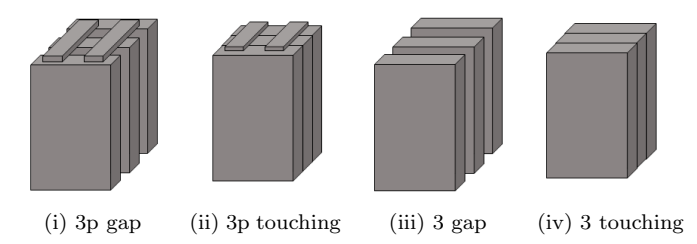


Fig. 8. Experimental testing configurations for three cells to parameterize the extended thermal model.

When three cells are placed next to each other, but separately powered, they transfer heat to each other and have less surface area exposed to air. So, we propose to revise the thermal model for the center cell to

$$\frac{dT_c}{dt} = \frac{\dot{Q}}{C_c} + \frac{T_s - T_c}{R_c C_c} 
\frac{dT_s}{dt} = \frac{T_c - T_s}{R_c C_s} + \frac{T_a - T_s}{R_{a,eq} C_s} + \frac{T_{s,l} - T_s}{R_s C_s} + \frac{T_{s,r} - T_s}{R_s C_s}$$
(12)

in which  $T_{s,l}$  and  $T_{s,r}$  are the surface temperatures of the cells to the left and right, respectively. This model introduces two new constants to the thermal model:  $R_s$ , which describes the thermal resistance to the transfer of heat between the cells, and  $R_{a,eq}$ , which is the equivalent thermal resistance to convection from the air based on the reduced surface area, defined as

$$R_{a,eq} = \frac{R_a}{1 - 2A_{loss,frac}} \tag{13}$$

in which  $A_{loss,frac}$  describes the effective fraction of the surface area on one side of a cell that is no longer exposed to convection. The center cell loses this area on both sides, while the outer cells only lose it on one side. We followed the prior procedure to find the optimal set of parameters for each case and the results are given in Table 3.

Table 3. Multi-cell thermal model parameters.

Test	$A_{loss,frac}$	$R_s$
(iii) Gap	0.3070	2.4639
(iv) Touching	0.3339	1.2524

Placing cells next to each other decreases the surface area exposed to free convection and introduces heat conduction between them, thus cells in the center of a battery pack have a larger temperature increase. The found lost surface area fractions,  $A_{loss,frac}$ , closely resemble the value based on geometry: 0.3227. Thus, when modeling cell packs, a valid assumption is that cells within a pack have only convection on their exposed faces. When the gap between the cells is smaller, there is less resistance to conduction, therefore the rate of heat transfer between the cells increases. Figure 9 compares the thermal model performance with identified parameters to data.

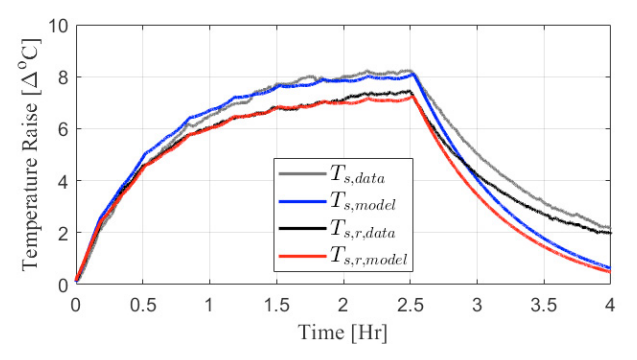


Fig. 9. Thermal model results for configuration with three separate cells with a gap (iii).

Note that multiple experiments are carried out for each configuration, however, for brevity only representative results are shown in this paper. Due to symmetry of heat transfer, the temperatures of the outer cells are equivalent, therefore only the surface temperature of the center cell,  $T_s$ , and the right cell,  $T_{s,r}$ , are shown.

#### 4.4 Bus Bar Thermal Modeling

In lumped parameter models of battery packs, the presence of bus bars is generally neglected as in Malik et al. (2018) or included with the cell to cell conduction as in Lin et al. (2014). To the best of our knowledge, only Fan et al. (2014) have included heat transfer through the bus bar, although their lumped parameter model is too simplistic since it describes the cell with only one temperature state. Moreover, their analysis is for a different cell chemistry.

To develop a model that captures the bus bar thermal effects, we propose to modify the two state thermal model in (12). Given that the cells are connected in parallel by bus bars at the terminals, it can be inferred that the bus bar transfers heat directly between the cores of the cells and dissipates heat to the environment. The bus bar's small mass and high thermal conductivity point to the assumptions that we can treat it as a path for energy transfer which has a uniform temperature that is equal to the core temperature. We will also make the assumption that each cell has an equal area of bus bar material which is exposed to convection. Therefore, the proposed model for the center cell's core and surface temperatures is

$$\begin{split} \frac{dT_c}{dt} &= \frac{\dot{Q}}{C_c} + \frac{T_s - T_c}{R_c C_c} + \frac{T_a - T_c}{R_{a,b} C_c} + \frac{T_{c,l} - T_c}{R_{c,b} C_c} + \frac{T_{c,r} - T_c}{R_{c,b} C_c} \\ \frac{dT_s}{dt} &= \frac{T_c - T_s}{R_c C_s} + \frac{T_a - T_s}{R_{a,eq} C_s} + \frac{T_{s,l} - T_s}{R_s C_s} + \frac{T_{s,r} - T_s}{R_s C_s} \; . \end{split}$$
(14)

The three new terms describe the heat dissipated to the air and the conduction through the bus bar between the center cell's core and the core of the cells to the left and right which have temperatures of  $T_{c,l}$  and  $T_{c,r}$ , respectively. This model introduces 2 new coefficients:  $R_{c,b}$ , which describes the thermal resistance to conduction from core to core through the bus bar, and  $R_{a,b}$ , which quantifies the resistance of the bus bar to convection from the air. These parameters are identified from experimental data using the prior framework and are provided in Table 4.

Table 4. Bus bar thermal model parameters.

Parameters				
$R_{c,b}$	3.2639  K/W	$k_b$	408.5 W/(m·K)	
$R_{a,b}$	48.2902  K/W	$A_{\text{surf},b}$	$1213.1 \text{ mm}^2$	

The computed thermal conductivity of the bus bar,  $k_b$ , confirms that the bus bar is primarily composed of copper. Furthermore, the computed bus bar surface area exposed to convection,  $A_{surf,b}$ , is equivalent to 65.5% of the total bus bar surface area.

Figure 10 depicts the error in the prediction of surface temperatures for a representative test with three cells connected in parallel. As seen in Fig. 10a, if the bus bar thermal effects are neglected and the model in (12) is used, the model will overestimate the surface temperature of both the center and right cell by around 10% or  $1^{\circ}C$  at steady state. Therefore, the proposed model consistently has a more accurate prediction.

The identified parameters for the model in (14) reveal that, interestingly, the bus bar creates a larger surface area for air convection, thus has cooling effects. Moreover, the bus

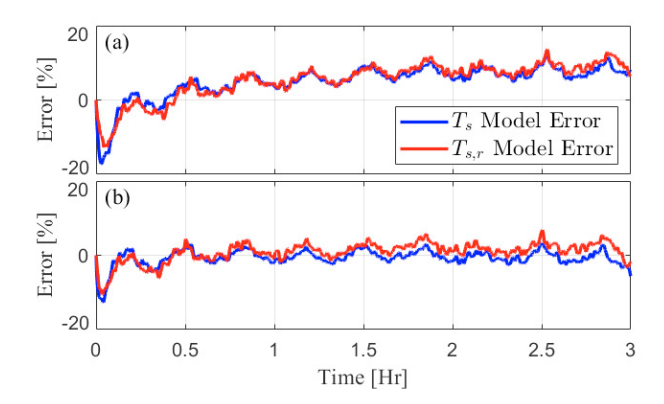


Fig. 10. Error in the prediction of surface temperature for the experiment with three parallel cells touching (ii) without (a) and with (b) including bus bar effects.

bar serves as a path for conduction between the cores of connected cells, which can contribute to a more uniform temperature distribution within a pack. These effects can be advantageous to battery cooling if the bus bar thermal effects are included in battery pack design.

Finally, it should be noted that the total heat conducted through the bus bars between two cells for this representative test was 1.128 kJ, compared to the 2.164 kJ of total heat transfer from direct cell-to-cell conduction. So, to extend a singe-cell thermal model to a battery pack, it is vital to include both the impacts of cells on each other, and the bus bars which connect them.

### 5. CONCLUSION

This paper proposed a thermal model for prismatic LFP cells, where each cell is represented by two states: one for surface temperature and another for the core temperature. We derived the model parameters using experimental data from thermal cycling. Our analysis highlighted the importance of reversible entropic heat generation in capturing the faster temperature dynamics within LFP cells. Furthermore, we showed that neglecting the thermal effects of the bus bar and merely extending a single-cell model to a cell pack will introduce prediction errors in the model. We proposed a method for capturing the bus bar role by integrating the conduction between the cell cores through the bus bar, and the heat dissipation from the bus bar surface to the surrounding air through convection.

Our future research direction will involve extending the developed model to more cells in parallel and series. Moreover, to further refine our understanding of heat transfer through the bus bar, we plan to include insulation to prevent cell-to-cell conduction in future experimental investigation. Finally, pre-cycling of one of the cells to elevate the temperature before packing the cells and observing the thermal dynamics will be another future research path.

## REFERENCES

Barbieri, M., Ceraolo, M., Lutzemberger, G., and Scarpelli, C. (2022). An electro-thermal model for lfp cells: calibration procedure and validation. *Energies*, 15(7), 2653.

Bazinski, S. and Wang, X. (2013). Determining entropic coefficient of the lfp prismatic cell at various tempera-

tures and charge/discharge states. ECS Transactions, 45(29), 85.

Bernardi, D., Pawlikowski, E., and Newman, J. (1985). A general energy balance for battery systems. *Journal of the electrochemical society*, 132(1), 5.

Camargos, P.H., dos Santos, P.H., dos Santos, I.R., Ribeiro, G.S., and Caetano, R.E. (2022). Perspectives on li-ion battery categories for electric vehicle applications: a review of state of the art. *International Journal of Energy Research*, 46(13), 19258–19268.

Chen, H., Zhang, T., Hua, Y., Gao, Q., Han, Z., Yang, K., Xu, Y., Liu, X., Xu, X., and Wang, S. (2023). Simulation study on the interaction between the battery module and busbar under typical driving conditions of electric vehicles. *Case Studies in Thermal Engineering*, 45, 103006.

Fan, G., Pan, K., Bartlett, A., Canova, M., and Rizzoni, G. (2014). Electrochemical-thermal modeling of li-ion battery packs. In *Dynamic Systems and Control Con*ference, volume 46193. American Society of Mechanical Engineers.

Forgez, C., Do, D.V., Friedrich, G., Morcrette, M., and Delacourt, C. (2010). Thermal modeling of a cylindrical lifepo4/graphite lithium-ion battery. *Journal of power sources*, 195(9), 2961–2968.

He, J., Hosen, M.S., Youssef, R., Kalogiannis, T., Van Mierlo, J., and Berecibar, M. (2023). A lumped electro-thermal model for a battery module with a novel hybrid cooling system. *Applied Thermal Engineering*, 221, 119874.

Hu, Y., Yurkovich, B.J., Yurkovich, S., and Guezennec, Y. (2009). Electro-thermal battery modeling and identification for automotive applications. In *Dynamic Systems* and Control Conference, volume 48937, 233–240.

Lin, X., Stefanopoulou, A.G., Siegel, J.B., and Mohan, S. (2014). Temperature estimation in a battery string under frugal sensor allocation. In *Dynamic Systems* and *Control Conference*, volume 46186, V001T19A006. American Society of Mechanical Engineers.

Malik, M., Mathew, M., Dincer, I., Rosen, M., McGrory, J., and Fowler, M. (2018). Experimental investigation and thermal modelling of a series connected lifepo4 battery pack. *International Journal of Thermal Sciences*, 132, 466–477.

Mendoza, S. and Fathy, H.K. (2014). Entropy coefficient and thermal time constant estimation from dynamic thermal cycling of a cylindrical lifepo4 battery cell. In *Dynamic Systems and Control Conference*, volume 46193. American Society of Mechanical Engineers.

Perez, H.E., Siegel, J.B., Lin, X., Stefanopoulou, A.G., Ding, Y., and Castanier, M.P. (2012). Parameterization and validation of an integrated electro-thermal cylindrical lfp battery model. In *Dynamic Systems and Control Conference*, volume 45318, 41–50. American Society of Mechanical Engineers.

Sheng, L., Su, L., and Zhang, H. (2019). Experimental determination on thermal parameters of prismatic lithium ion battery cells. *International Journal of Heat and Mass Transfer*, 139, 231–239.

Wang, J., Liu, P., Hicks-Garner, J., Sherman, E., Soukiazian, S., Verbrugge, M., Tataria, H., Musser, J., and Finamore, P. (2011). Cycle-life model for graphite-lifepo4 cells. *Journal of power sources*, 196(8), 3942–3948.